Fault behaviour of bipolar overhead line based HVDC grids

P. Torwelle[#], A. Bertinato[#], B. Raison[#], T.D. Le[#†], M. Petit[#†]*

[#]SuperGrid Institute, Villeurbanne, France, pascal.torwelle@supergrid-institute.com
**Univ. Grenoble Alpes, CNRS, Grenoble INP*, G2Elab, F-38000 Grenoble, France*
[†]CentraleSupelec, CNRS, GeePs, F-91192 Gif sur Yvette, France

Keywords: Bipolar grid, Overhead line, Fault analysis, Modal domain, HVDC.

Abstract

This paper provides a fault analysis of bipolar overhead line based HVDC grids using HB-MMC converters. The impacts of fault type and fault resistance are shown and the physical behaviour of the transient fault return current is explained. A transformation in modal quantities enables a decoupling of the measured phase currents and voltages. The results are presented in a point-to-point HVDC grid for both phase and modal quantities. It is shown that fault analysis in the modal domain is an auspicious method for fault detection and faulty line discrimination.

1 Introduction

High voltage direct current (HVDC) grids are advantageous for renewable energy transmission from often remote areas to metropolitan regions in order to relieve existing AC grids. Most of nowadays planned HVDC systems will use cables for power transmission, since the right of way for overhead lines (OHL) is difficult to obtain. However, existing AC lines could be upgraded and subsequently used in HVDC systems, which would be an interesting solution because of both simplicity and cost efficiency [1].

In order to develop a reliable protection strategy and to ensure a resilient HVDC grid operation, the investigation of the system behaviour under fault condition is mandatory. In previous studies [2–4], the fault behaviour of overhead lines in bipolar DC grids has been analysed with different objectives. In [2], transient overvoltages on the healthy pole during a Pole-to-Ground fault are investigated. Reference [3] analyses the frequency dependency of OHL during faults. In [4], a symmetrical component decomposition is proposed in order to analyse faults in DC grids including a dedicated metallic return (DMR). Reference [5] analyses the fault characteristics of cable systems in phase and modal domain.

This study aims to analyse different fault types such as Pole-to-Ground (PtG), Pole-to-Pole (PtP) and Pole-to-DMR (PtD) faults in order to enable fault detection and discrimination. The studies have been carried out for a bipolar Point-to-Point grid with HB-MMC converters. The results are shown in phase and in modal quantities. Starting with a simple system of two conductors, a ground wire (GW) and then a DMR are added in order to show their effects.

* Institute of Engineering Univ. Grenoble Alpes

2 Travelling wave theory in phase and modal domain

The fault behaviour of a multi-conductor transmission line can be analysed in phase and modal quantities [6]. The latter decomposes the multi-conductor system into independent uncoupled modes as this can facilitate the physical understanding. In the following section, both approaches are briefly introduced.

2.1 Phase quantities

In the phase domain, differential equations can be applied for multi-conductor electromagnetic transient (EMT) studies:

$$-\frac{d\mathbf{v}}{dx}=\mathbf{L}\frac{d\mathbf{i}}{dt}+\mathbf{R}\,\mathbf{i} \tag{1}$$

$$-\frac{d\mathbf{i}}{dx}=\mathbf{C}\frac{d\mathbf{v}}{dt}+\mathbf{G}\,\mathbf{v} \tag{2}$$

$\mathbf{v}$ and $\mathbf{i}$ are column vectors of voltage and current respectively. $\mathbf{L}$, $\mathbf{R}$, $\mathbf{C}$ and $\mathbf{G}$ are matrices which represent respectively inductance, resistance, capacitance and conductance values of the system. The matrices are quadratic and consist of non-diagonal elements since the conductors are coupled across mutual inductance and shunt admittance. In a further step, telegrapher's equations can be applied:

$$\frac{d^2\mathbf{v}}{dx^2}=\mathbf{Z}\,\mathbf{Y}\,\mathbf{v} \tag{3}$$

$$\frac{d^2\mathbf{i}}{dx^2}=\mathbf{Y}\,\mathbf{Z}\,\mathbf{i} \tag{4}$$

$\mathbf{Z}$ is the serial impedance matrix and $\mathbf{Y}$ is the shunt admittance matrix.

2.2 Modal quantities

Modal quantities can be obtained by transforming Equations (3) and (4) using transformation matrices $\mathbf{T}_i$ and $\mathbf{T}_v$:

$$\frac{d^2\mathbf{v}_m}{dx^2}=\mathbf{T}_v^{-1}\mathbf{Z}\,\mathbf{Y}\,\mathbf{T}_v\,\mathbf{v}_m \tag{5}$$

$$\frac{d^2\mathbf{i}_m}{dx^2}=\mathbf{T}_i^{-1}\mathbf{Y}\,\mathbf{Z}\,\mathbf{T}_i\,\mathbf{i}_m \tag{6}$$

The transformation matrices $\mathbf{T}_i$ and $\mathbf{T}_v$ can be deduced by solving the eigenvector/eigenvalue problem of the matrix product $\mathbf{Y}\,\mathbf{Z}$ and $\mathbf{Z}\,\mathbf{Y}$ respectively. More detailed explanation about the modal approach is provided in [6]**.** Modal voltages and currents can be transformed using Equations (7) and (8).

$$\mathbf{v}_m=\mathbf{T}_v^{-1}\mathbf{v} \tag{7}$$

$$\mathbf{i}_m=\mathbf{T}_i^{-1}\mathbf{i} \tag{8}$$

The modal impedance and admittance matrix is obtained by:

$$\mathbf{Z}_m=\mathbf{T}_u^{-1}\mathbf{Z}\,\mathbf{T}_i \quad (9)$$

$$\mathbf{Y}_m=\mathbf{T}_i^{-1}\mathbf{Y}\,\mathbf{T}_u \quad (10)$$

The *n* conductor system is now transformed in *n* independent modes. Characteristic impedance and propagation constant of each mode can be found by solving the scalar Equations (11) and (12).

$$Z_{c\,m}=\sqrt{\frac{Z_m}{Y_m}} \quad (11)$$

$$\gamma_m=\sqrt{Z_m\,Y_m} \quad (12)$$

3 Fault analysis of OHL based HVDC grids

In this main section, the fault behaviour of bipolar HVDC grids based on OHL is analysed. In a first step, the grid topology is specified, defining components, parameters, OHL topologies and fault cases. Afterwards, the physical effects are explained while increasing the number of conductors step by step and showing its effects for different fault types. Simulations are carried out in EMTP-RV. The results are illustrated both in phase and modal quantities.

3.1 Grid topology

The fault analysis is carried out in a bipolar point-to-point HVDC grid with Half-Bridge Modular-Multilevel-Converters (HB-MMC). HB-MMC do not have a current breaking capability but in order to protect the IGBT modules, the blocking current limit is usually set to 2 p.u. of their rated current. The grid topology is shown in Figure 1 and the parameters of each converter are listed in Table 1.

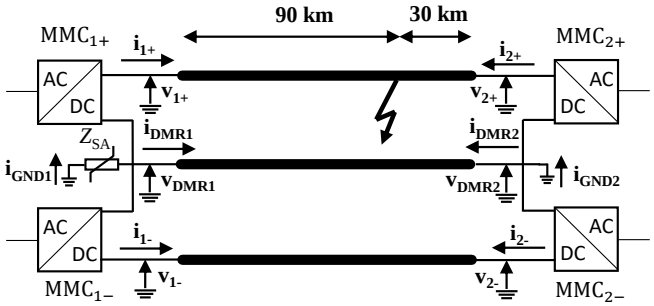

Figure 1 Grid topology

Description	Parameter	Unit	Value
Rated power	S_{MMC}	MVA	500
Rated voltage	V_{DC}	kV	±320
Arm inductance	L_{arm}	mH	16
Arm resistance	R_{arm}	Ω	0.1

Table 1 MMC Parameters

The total conductor length is l=120 km. The fault location for this study is at 90 km distance to MMC_{1+} and at 30 km distance to MMC_{2+}. The pylon architecture is shown in Figure 2.

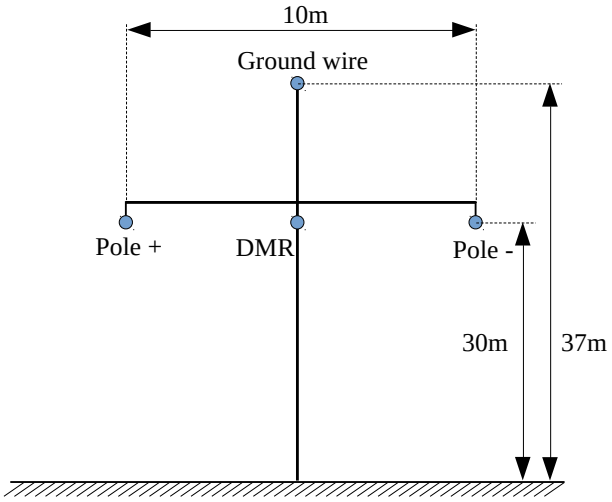

Figure 2 Pylon architecture

The bipolar system consists of a positive and negative conductor, a DMR and a GW. The DMR is employed to avoid complications due to ground current when one pole is out of service [7]. The GW is placed above the conductors to protect from lightning strokes. It is grounded at every pylon. The pylon grounding resistance is set to R_{Pylon}=6 Ω.

Comparing conductor characteristics, the per unit length resistance of the GW is higher and the diameter is smaller. The parameters are given in Table 2. The ground return resistivity is set to 100 Ω m [3]. For the EMT studies, a wideband model is used.

Conductor	DC resistance [Ω/km]	Diameter [cm]
Pole ± / DMR	0.0224	4.775
GW	3.65	0.954

Table 2 Conductor parameters

HVDC faults can be classified into three main fault types: PtG fault, PtD fault and PtP fault [7]. For the former one, half of rated power can still be provided during fault by the healthy pole because at least one pole and the DMR are not impacted. The two latter fault cases could lead to a total power flow interruption. In addition, especially for PtG faults, the fault resistance may have different values between several Ohms and several hundreds of Ohms. In this study, low and high resistance faults between R_f=0.1-100 Ω are analysed in order to reinforce physical understanding of fault current behaviour [8].

3.2 Two conductor configuration

In a first step, a simple two conductor system which consists of a positive and a negative conductor without GW and DMR is considered in the Point-to-Point HVDC grid. A positive PtG fault is applied with fault resistance variation (R_f=0.1-10-100 Ω). The simulation results for both MMC stations are shown in Figure 3. The time frame is chosen to be 5 ms, since the first few milliseconds are important for fault detection and discrimination.

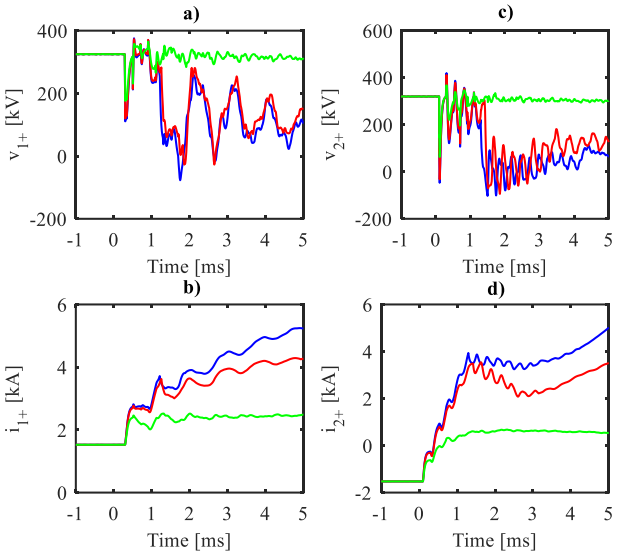

Figure 3 Voltages and currents of MMC_{1+} (a,b) and MMC_{2+} (c,d) during positive PtG fault;
R_f=0.1Ω (blue), R_f=10Ω (red), R_f=100Ω (green)

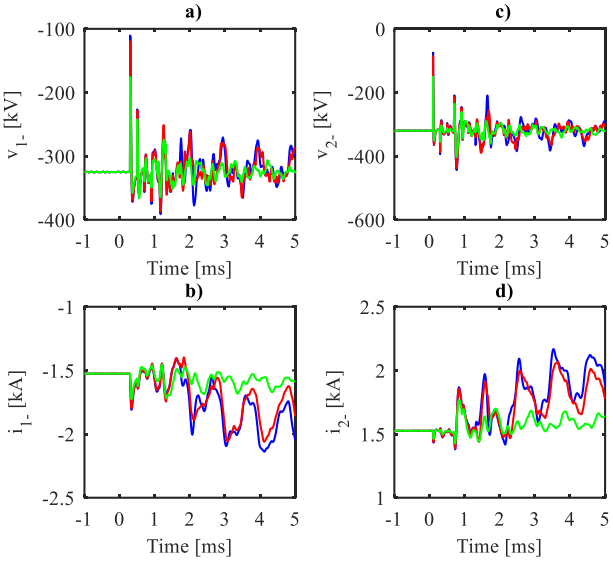

Figure 4 Voltages and currents of MMC_{1-} (a,b) and MMC_{2-} (c,d) during positive PtG fault;
R_f=0.1Ω (blue), R_f=10Ω (red), R_f=100Ω (green)

The arrival of the initial propagation wave provokes a rise of current and a voltage drop at both line ends. The amplitude depends on the surge impedance of the line and on the fault resistance. For low fault resistances (R_f=0.1-10 Ω), the current rises until MMC blocking at 2 p.u. of rated current, whereas for high resistance faults (R_f=100 Ω), the current stays under the 2 p.u. threshold.
In the first few milliseconds before blocking, the fault current contribution comes from the converter and positive line-to-ground capacitor discharge. After blocking, the MMC switches in diode rectifier mode and the main fault current is fed by AC sources. In fact, the blocking has an important impact on the voltage of the converter stations (Figure 3a,c). The first propagation wave leads to a drop of converter voltages. With ongoing reflections, the amplitude declines. The blocking of the MMC is an additional event which impacts the voltage and current wave reflections. Hence, a second voltage drop occurs for low resistance faults at about t=1.3 ms for v_{1+} and at t=1.4 ms for v_{2+}, whereas the voltage for high resistance faults stays close to nominal voltage, as the MMC does not block.

In Figure 4, the healthy pole voltages and currents of both converter stations are shown. For high and low resistance faults, the rise of current on the faulty pole induces high voltage oscillation in the healthy pole due to mutual inductance (a,c). The currents show oscillations as well, which can be explained by the mutual coupling and by control effects intervening due to voltage instability after about 2 ms.
The conductors are coupled due to mutual inductance, so that the fault event has an important impact on the healthy pole. This remark is only valid for OHL, since the mutual coupling between the conductors in cable configurations is very low.

The transformation of the voltages and currents from both stations into modal quantities can be achieved by using the following transformation matrix:

$$T_i^{-1}=T_u^{-1}=\frac{1}{\sqrt{2}}\begin{bmatrix}1 & 1\\ 1 & -1\end{bmatrix} \quad (13)$$

Exemplary, the modal transformation of the phase currents of MMC_1 is shown in equation (14).

$$\begin{bmatrix}i_{1\,m0}\\ i_{1\,m1}\end{bmatrix}=\frac{1}{\sqrt{2}}\begin{bmatrix}1 & 1\\ 1 & -1\end{bmatrix}\begin{bmatrix}i_{1+}\\ i_{1-}\end{bmatrix} \quad (14)$$

Mode 0 can be understood as a ground return mode, whereas Mode 1 is an aerial mode. The path of each modal current is depicted in Figure 5.

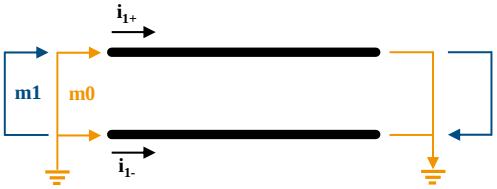

Figure 5 Path of modal currents for two conductors

In Figure 6, the results for modal currents of MMC_1 during a positive PtG fault (a,b), a negative PtG fault (c,d) and a PtP fault (e,f) are shown.
The ground return mode currents differ depending on the fault type. For a positive PtG fault the currents are of positive value, whereas the currents for a negative PtG fault have a negative sign. This is valid for low resistance faults as well as high resistance faults. For a PtP fault, the ground return mode current remains zero, since there is no current flowing through the ground.
Regarding the aerial mode, the current before fault occurrence depends on the load flow of the grid. In this case, it is positive. For both positive and negative PtG faults, the current rises in the same way. A PtP fault leads to a high current of more than 4.5 kA after the first propagation wave.

The mentioned characteristics of the modal currents are beneficial for fault detection and fault type discrimination, since the ground return mode current remains zero before fault occurrence independent from the load flow when a balanced system is considered. Hence, the sign of the ground return mode current can be used to discriminate the faulty pole.

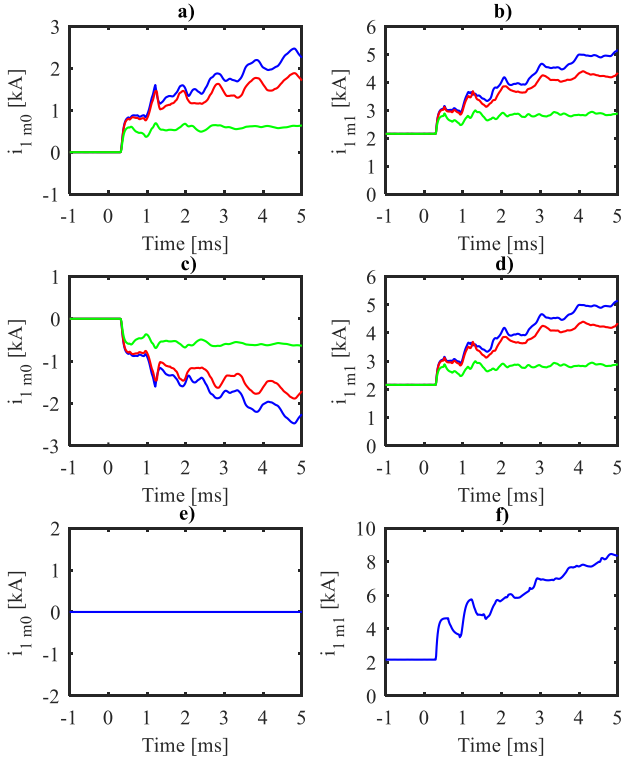

Figure 6 Modal currents of MMC_1 for a positive (a,b) and negative (c,d) PtG fault and a PtP fault (e,f); R_f=0.1Ω (blue), R_f=10Ω (red), R_f=100Ω (green)

3.3 Two conductor plus GW configuration

The ground wire is an additional line which is used to protect the conductors from lightning strokes. It is grounded at every pylon and at the converter stations. When a PtG fault occurs, two fault current return paths are possible. In Figure 7, the path of the fault current i_f is shown. The fault current could return through the ground (i_{GND}) or through the GW (i_{GW}). Thus, the ground wire becomes a potential conductor of return current besides the ground.

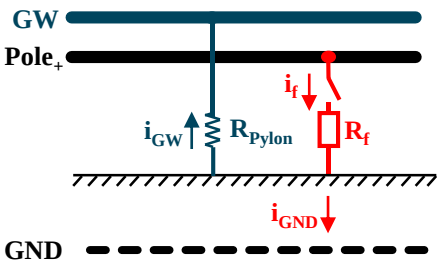

Figure 7 Possible fault current paths

In Figure 8 the division of the fault current i_f (green) is shown. Regarding the initial fault current peak (1480 A), an important part flows through the ground (1250 A) and only a small part flows though the ground wire (230 A). This can be explained by the discharge of capacitance between both the Conductor-GND and Conductor-GW. The capacity of the former one is far more important, which explains the higher value of initial fault current in the ground. For further propagation waves, the return current flowing through the GW remains small because of a high damping of the GW current. The ground return current i_{GND} rises proportional to the fault current i_f. For the modal transformation, the same matrix as in Equation (14) can be applied. The results are similar to those, shown in Figure 6.

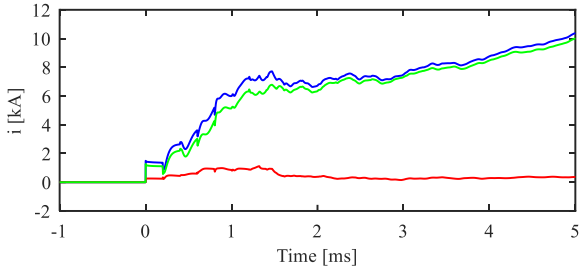

Figure 8 i_f (blue) and return current subdivision: i_{GND} (green) and i_{GW} (red); R_f=0.1Ω

3.4 Two conductor plus GW and DMR configuration

The full system consists of the positive and the negative conductor, a GW and a DMR according to Figure 2. In order to avoid current flowing through the ground during normal operation, one converter station is solidly grounded and the other one is grounded via a surge arrester. To limit the metallic return potential deviation from earth, the surge arrester protective level is set to $v_{SA,ref}$ = 30 kV.

In case of a PtG fault, after initial transients the fault current returns by the grounding of the two converter stations. The ground return currents of both stations i_{GND1} and i_{GND2} are shown in Figure 9. The rise of current depends on both the distance of each converter station to the fault and on the surge arrester resistance.

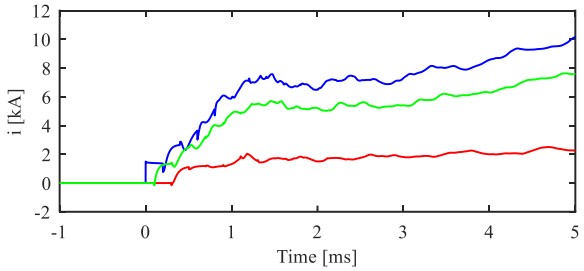

Figure 9 Fault current i_f (blue) and ground return current i_{GND1} (red) and i_{GND2} (green)

In Figure 10, the voltages and currents of both converter stations are shown during a positive PtG fault. Compared to the results obtained in a simple two conductors system, the current contribution is of similar shape. The voltage of the DMR at MMC_1 is shown in (e). At fault occurrence, after the first positive peak linked to the propagation of the fault related wave, the voltage level drops close to surge arrester protective level. Hence, the surge arrester begins conducting current and lets the

fault current pass. Due to the voltage difference between the groundings of the two converter stations, a current of negative sign is flowing through the DMR.

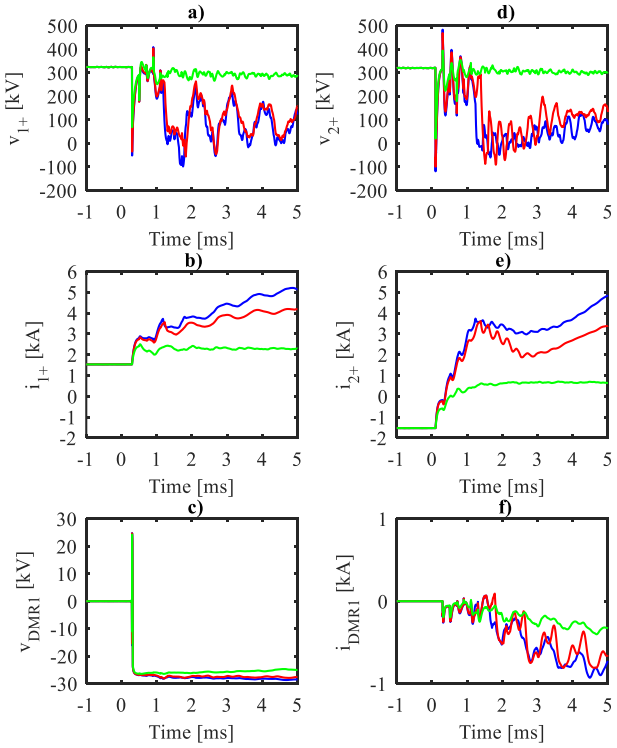

Figure 10 Voltage and current of MMC_{1+} (a,b), MMC_{2+} (d,e) and DMR1 (c,f) during positive PtG fault; R_f=0.1Ω (blue), R_f=10Ω (red), R_f=100Ω (green)

For this configuration, a PtD fault and a PtP fault are considered additionally. In Figure 11 results for the MMC_1 during a PtP fault are depicted. The voltage transients are characterized by propagation waves of almost twice the rated voltage which corresponds to the voltage difference of both poles before the fault. The voltage waves show little damping since this fault type is based on aerial mode characteristics. The currents i_{1+} and i_{1-} are of opposite sign, so that both currents are rising but in opposite direction. The DMR is not directly concerned. Only voltage oscillations related to mutual inductance appear.

In Figure 12, the behavior during a PtD fault is shown. The DMR is directly connected to the positive pole, which provokes a voltage and current wave propagation between fault and line ends. The voltage wave amplitudes are high compared to the rated voltage of the surge arrester. This causes an irregular change of polarity.
In this fault case, the fault current is contributed by MMC_{1+} and MMC_{2+} and obviously returns through the DMR, so that the current of each converter station is of negative value. For a negative PtD fault, i_{DMR1} becomes positive.

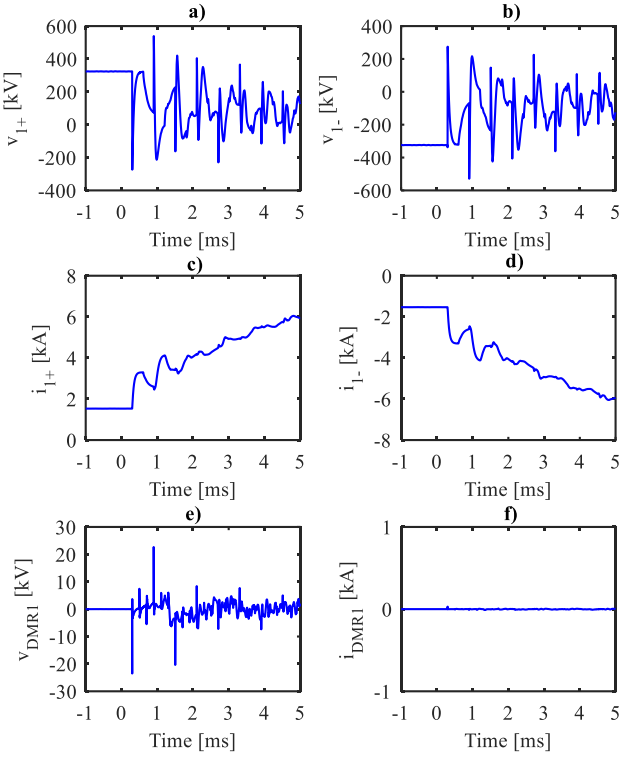

Figure 11 Voltage and current of MMC_{1+} (a,c), MMC_{1-} (b,d) and DMR (e,f) during a PtP fault

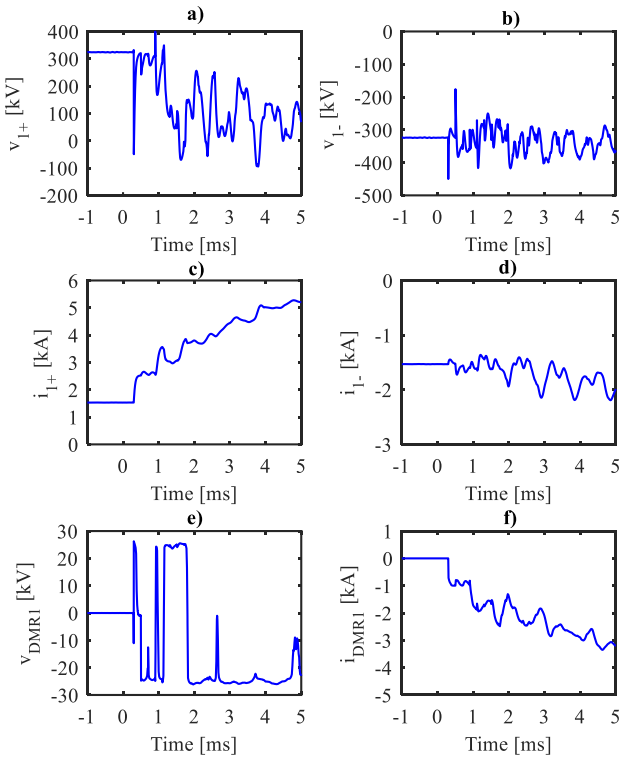

Figure 12 Voltage and current of MMC_{1+} (a,c), MMC_{1-} (b,d) and DMR (e,f) during a PtD fault

The transformation of the pole currents and the DMR current of MMC_1 into modal quantities leads to three modes, whereof

one ground return mode (m0) and two aerial modes (m1, m2) according to Equation (15). The path of each modal current is shown in Figure 13. Aerial mode current $i_{1\,m1}$ flows through the positive pole conductor and returns by the negative one. The aerial mode current $i_{1\,m2}$ flows through the DMR and returns by the two poles. $i_{1\,m0}$ returns by the ground.

$$\begin{bmatrix} i_{1\,m0} \\ i_{1\,m1} \\ i_{1\,m2} \end{bmatrix} = \begin{bmatrix} 0.58 & 0.58 & 0.58 \\ 0.71 & -0.71 & 0 \\ -0.38 & 0.38 & 0.85 \end{bmatrix} \begin{bmatrix} i_{1+} \\ i_{1-} \\ i_{DMR} \end{bmatrix} \quad (15)$$

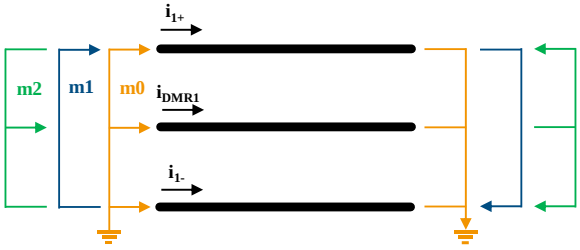

Figure 13 Path of modal currents for three conductors

The fault analysis for the different fault types can be carried out in modal quantities as well. Figure 14 shows the mode currents for a positive (blue) and negative (red) PtG fault (a-c), for a PtP fault (d-f) and for a positive (blue) and negative (red) PtD fault (g-i).

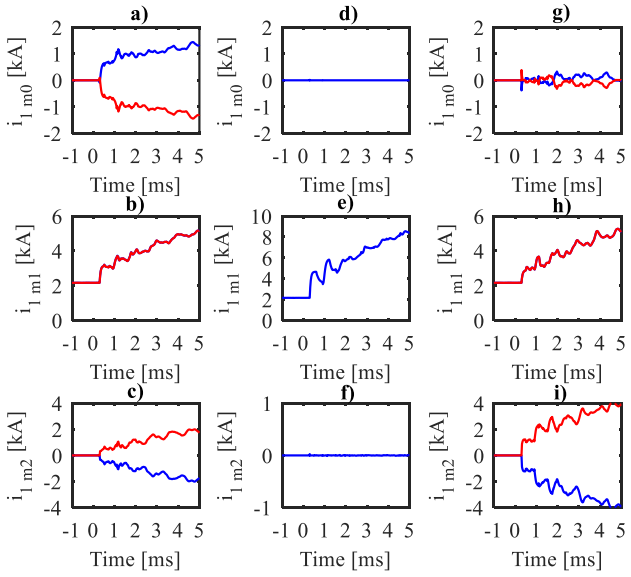

Figure 14 Modal currents of MMC_1 during PtG fault (a-c), PtP fault (d-f) and PtD fault (g-i)

In steady state operation, the ground return mode current $i_{1\,m0}$ and the aerial mode current $i_{1\,m2}$ are equal to zero. In contrast, the other aerial mode current is of positive value: $i_{1\,m1} = 2165$ A.

For PtG faults, $i_{1\,m0}$ is rising in positive or negative direction depending on the faulty pole, whereas the rise of $i_{1\,m1}$ does not depend on the faulty pole. $i_{1\,m2}$ declines for a positive PtG fault but rises when the negative pole is faulty.

During a PtP fault, $i_{1\,m0}$ and $i_{1\,m2}$ remain zero, whereas $i_{1\,m1}$ rises. For a PtD fault, the ground return mode current remains close to zero but $i_{1\,m1}$ is rising. $i_{1\,m2}$ declines if the positive pole is faulty and rises for a faulty negative pole.

4 Conclusion

A fault analysis of an overhead line based HVDC system has been carried out for different fault types. The results have been presented for different conductor configurations in phase domain, as well as in modal domain.

When overhead transmission lines are used, fault events provoke a slow rise of current on the faulty line and oscillations with high derivatives on the healthy line due to mutual inductance. Therefore, care should be taken by using phase quantities for fault detection and discrimination. However, the modal domain enables to decouple the system into a ground return mode and aerial modes. Especially the ground return mode provides interesting characteristics to determine the faulty pole since the sign of the ground return mode current enables to distinguish the faulty pole.

Acknowledgements

This work has been carried out at the SuperGrid Institute, an institute for the energy transition (ITE). It is supported by the French government under the frame of "Investissements d'avenir", No. ANE-ITE-002-01. This work is supported in part by EU H2020 PROMOTioN project, under Grant Agreement No. 691714.

References

[1] J. Lundquist et al., "Cigré 583: Guide to the conversion of existing AC lines to DC operation." Cigré.

[2] E. W. Kimbark, "Transient Overvoltages Caused by Monopolar Ground Fault on Bipolar DC Line: Theory and Simulation," *IEEE Trans. Power Appar. Syst.*, vol. PAS-89, no. 4, pp. 584–592, Apr. 1970.

[3] A. Wasserrab and G. Balzer, "The significance of frequency-dependent overhead lines for the calculation of HVDC line short-circuit currents," *Electr. Eng.*, vol. 97, no. 3, pp. 213–223, Sep. 2015.

[4] N. H. van der Blij, L. M. Ramirez-Elizondo, M. T. J. Spaan, and P. Bauer, "Symmetrical Component Decomposition of DC Distribution Systems," *IEEE Trans. Power Syst.*, vol. 33, no. 3, pp. 2733–2741, 2018.

[5] D. Loume, M. Nguyen Tuan, A. Bertinato, B. Raison, "DC cable modelling and High Voltage Direct Current grid grounding system," in *9th International Conference on Insulated Power Cables JICABLE 2015*, 2015

[6] C. R. Paul, "Decoupling the multiconductor transmission line equations," *IEEE Trans. Microw. Theory Tech.*, vol. 44, no. 8, pp. 1429–1440, Aug. 1996.

[7] S. Beckler, J. Lehner, A. Arnold, A. K. Kamga, K. Frey, and K. Rudion, "DC Fault Currents for FB-MMC HVDC with Bipolar Configuration," in *International ETG Congress 2015*, 2015, pp. 1–6.

[8] J. De Andrade Suárez and E. Sorrentino, "Typical expected values of the fault resistance in power systems," in *2010 IEEE/PES Transmission and Distribution Conference and Exposition: Latin America, T and D-LA 2010*, 2010, pp. 602–609.